Physics Letters B 704 (2011) 461–466

Contents lists available at SciVerse ScienceDirect

Physics Letters B

www.elsevier.com/locate/physletb

Measurement of the antiproton–nucleus annihilation cross section at 5.3 MeV

A. Bianconi [a,b], M. Corradini [a,b], M. Hori [c,d], M. Leali [a,b], E. Lodi Rizzini [a,b,*], V. Mascagna [a,b], A. Mozzanica [a,b,1], M. Prest [e,f], E. Vallazza [g], L. Venturelli [a,b], N. Zurlo [a,b]

[a] Dipartimento di Chimica e Fisica per l'Ingegneria e per i Materiali, Università di Brescia, 25133 Brescia, Italy
[b] Istituto Nazionale di Fisica Nucleare Gruppo Collegato di Brescia, 25133 Brescia, Italy
[c] Max-Planck-Institut für Quantenoptik, Hans-Kopfermann-Strasse 1, D-85748 Garching, Germany
[d] Department of Physics, University of Tokyo, 7-3-1 Hongo, Bunkyo-ku, Tokyo 113-0033, Japan
[e] Istituto Nazionale di Fisica Nucleare Sezione di Milano Bicocca, Italy
[f] Università degli Studi dell'Insubria, Italy
[g] Istituto Nazionale di Fisica Nucleare Sezione di Trieste, Trieste, Italy

ARTICLE INFO

Article history:
Received 11 July 2011
Received in revised form 7 September 2011
Accepted 16 September 2011
Available online 22 September 2011
Editor: M. Doser

Keywords:
Antiproton annihilations
Low energies
Nuclear reactions

ABSTRACT

Antiproton annihilation cross sections on medium-heavy and heavy nuclear targets are measured for the first time at 5.3 MeV kinetic energy at the Antiprotons Decelerator facility of CERN. The results agree with the expected behavior from the black-disk model with the Coulomb corrections.

1. Introduction

The LEAR (Low Energy Antiproton Ring) era has left us with a rich set of measurements of annihilation cross sections (here after denoted as σ) for unpolarized antinucleons on nuclear targets at energies as low as ≈ 1 MeV (≈ 40 MeV/c $\bar{p}$ lab momentum), see Ref. [1–5].

An important point is to predict which mass and energy dependencies one should expect in the MeV and sub-MeV regions of the $\bar{p}$ energy. For classification purposes, we may consider two opposite (limit) regimes for annihilations: the semiclassical and the quantum S-wave-dominated regime [6]. On general grounds we could use the number of involved partial waves to establish a rough borderline between the two regimes. For heavy nuclear targets it is not clear whether a kinematical regime dominated by the S-wave exists at all.

For large nuclear radii and short enough wavelengths we may imagine a semiclassical regime with black disk, energy-independent cross sections of the kind $\pi R^2 \sim A^{2/3}$ (A is the target mass number) and some additional corrections, see Ref. [7]. At small energies ($\bar{p}$ lab momentum less than 100 MeV/c for light nuclei and several hundreds of MeV/c for heavy nuclei [8]), the cross sections will be enhanced by the Coulomb force which focus the classical projectile trajectories toward the nuclear interaction volume. The effect of Coulomb focusing increases with increasing nuclear charge, and prevents the number of involved partial waves from becoming small at non-infinitesimal energies. A semiclassical evaluation with the inclusion of the Coulomb interaction into the black-disk model [7] gives for the reaction cross section $\sigma_r = \pi R^2[1 + \frac{Ze^2(m+M)}{4\pi\epsilon_0 ERM}]$ where E is the kinetic energy in the laboratory system of the antiproton of mass m, M is the mass of the target and R is the equivalent radius that represents the $\bar{p}$-nucleus interaction; at very low energies $\sigma = \sigma_r \sim ZR \sim ZA^{1/3}$.

Moreover, it is well known that antineutron–nuclei annihilation cross sections are in good agreement with the $A^{2/3}$ behavior even at ≈ 60 MeV/c [9,10].

Summarizing, the LEAR era has left us some interesting and unsettled issues on the behavior of the in-flight annihilations of antinucleons on not-light nuclei at small energies.

At the present time the only existing source of low energy antiprotons is the Antiproton Decelerator (AD) [11], the successor of LEAR at CERN. The ASACUSA Collaboration has planned to perform measurements of the antiproton–nuclei annihilation cross section

* Corresponding author at: Dipartimento di Chimica e Fisica per l'Ingegneria e per i Materiali, Università di Brescia, 25133 Brescia, Italy.
E-mail address: lodi@bs.infn.it (E. Lodi Rizzini).

[1] Presently at PSI.

0370-2693
doi:10.1016/j.physletb.2011.09.069

down to the region of the tens of keV. In order to achieve these very low energies at the AD where the antiproton beam is pulsed, a purpose-built apparatus has been at first used at the MeV region.

In this Letter we present the results of the search for the values of $\bar{p}$-nuclei annihilation cross sections at 5.3 MeV on Mylar, Ni, Sn and Pt targets.

2. Experimental setup

The antiproton bunch from AD is normally 100 ns long, contains $(2\text{–}4)\times 10^7$ $\bar{p}$s of momentum $p = 100$ MeV/c (corresponding to an energy of 5.3 MeV) with a momentum spread of $\Delta p/p = 0.01\%$ and an emittance of $(1\text{–}2)\pi$ mm mrad. The fast pulsed extraction of the antiproton beam, in contrast to the slow extraction at LEAR, represents the main difficulty in performing a measurement of antiproton annihilation cross section at AD. The repetition rate is of the order of 0.01 Hz.

To optimize the beam use, ASACUSA has performed both accurate settings of the AD beam and a particular design of the experimental setup.

Concerning the AD beam optimization, the so-called "multiple extraction" option was used. Radio frequency cavities first bunched the 100-MeV/c antiprotons circulating in the AD into six beam pulses, which were distributed equidistantly around the 190-m-circumference of the AD. Each pulse contained around 5×10^6 antiprotons. These were sequentially extracted to the experiment every 2.4 s, using a kicker magnet installed in the AD. The duration of the pulsed magnetic field applied to the kicker was adjusted such that the antiproton pulses arriving at the experiment were around 40–50 ns long. A series of retractable beam scrapers were installed in the vacuum chamber of the AD. These were moved within a few centimeters of the beam axis, so that they effectively became an iris which removed the unwanted halo part of the beam circulating in AD. In this way, the diameter of the antiproton beam arriving at the experiment was reduced (see later).

The experimental setup was designed with a particular care to avoid contaminations from the $\bar{p}$ annihilations not occurring on the target. A sketch of the experimental setup is drawn in Fig. 1. It is quasi-axial symmetrical around the $\bar{p}$ beam and consists of a vessel ($l = 100$ cm, $\phi = 15$ cm) containing a thin solid target surrounded by a vertex detector. The vessel was directly connected to the AD beam pipe without any material along the $\bar{p}$ beam before the target. To reduce the Rutherford scattering background a second larger vessel ($l = 120$ cm, $\Phi = 60$ cm) was joined to the first one. In addition it was as long as possible (a compromise with the mechanical constrains) to reduce contaminations from the $\bar{p}$ annihilating on the end wall, where a beam counter was placed to monitor the $\bar{p}$ beam intensity. The beam counter consists of 1 cm thick Bicron BC408 plastic scintillator (20×10 cm^2) with Hybrid Photo-Detector (HPD) readout. It measures the total charge deposited by the products from the antiproton annihilation on the end wall of the target vessel. Since the device was not calibrated, only the relative numbers of the injected antiprotons were measured.

To detect the annihilation events on the targets we realized a vertex detector [12,13] which is able to reconstruct the tracks of the charged pions emitted in the $\bar{p}$ annihilation by means of scintillating fibers (Bicron BCF10 Multiclad, coated with Extra Mural Absorber to reduce the crosstalk between adjacent fibers). It consists of two cylindrical shells (50 cm long with an external radius of 11.5 and 15 cm, respectively) coaxially with the $\bar{p}$ beam. Each shell contains 3 double-layers of scintillating fibers: one is parallel to the $\bar{p}$ beam, the other two are placed to form helices with ± 20 degrees. In this way we can get 2 points of each track crossing the detector, resolving the ambiguities when several tracks coexist. Every double-layer is realized by scintillating fibers of 1 mm diameter which are collected in groups of 4 neighboring fibers. Each group is connected to an anode of a 64 channels multianode PMT (H7546B by HAMAMATSU KK). The signals from the PMTs are amplified, shaped and discriminated by VLSI ASICs (Application Specific Integrated Circuit) manufactured by Gamma Medica-Ideas (VA64TAP2.1 and LS64_2) and then are sent to a Cyclone II FPGA (Field Programmable Gate Array) by Altera for time sampling. The sampled data are sent to the VME-based DAQ. The total number of channels is 2688 for a total length of fibers of almost 10 km. The time resolution of the DAQ chain was measured on a prototype and resulted to be of the order of some nanoseconds with an efficiency of 94%.

The design of the apparatus has been guided by Monte Carlo simulations based on Geant 3.21 and a combinatorial algorithm for the vertex determination. In the simulation program a phase space generator for antiproton–proton annihilation is inserted with the branching ratios taken from Ref. [14].

The vertex is determined by considering all the possible straight lines passing through 2 hits (one on the inner shell of the detector, the other on the external one). Some of these lines correspond to charged pion tracks, while the others are fake tracks coming out from the combinatorial logic of the used algorithm. For each couple of tracks the point of the minimal distance between them is measured. The average position of these points is then evaluated to determine the final annihilation vertex. The efficiency in the vertex determination is 80% for the simulated antiproton–proton annihilations occurring at the center of the apparatus assuming no inefficiency in the fiber detection system. The spatial resolutions is 0.4–0.5 cm on the z-coordinate (z-axis is along the $\bar{p}$ beam direction) and 0.3–0.4 cm on the x, y transverse coordinates.

Since the tracks coming from different annihilations can be disentangled only if few annihilations occur per bunch (the critical number depends on the length of the bunch: in a time range of 10 ns only 2–3 vertices are precisely reconstructed), the thickness of the target must be very thin. We have sputtered metallic disks (5 cm in diameter) on Mylar foils (12 cm in diameter and 860 ± 20 nm in thickness). We used nickel, tin and platinum targets with a suitable thickness in order to produce annihilation events numbers comparable with the ones from Mylar assuming an $A^{2/3}$ law for σ. The Mylar in turn constitutes a target with an A-number similar to the carbon one (see later). The actual thicknesses of the metallic targets have been measured by means of Rutherford backscattering technique (RBS) and their values are 240 ± 10 nm, 400 ± 40 nm, 115 ± 5 nm for Ni, Sn and Pt respectively [15].

We positioned one target at a time along the $\bar{p}$ beam near the end of the first vessel: the changing and positioning of the targets was done very quickly without opening the target vessel by means of a rotary linear multi-motion system which moved the selected target on the $\bar{p}$ beam from the parking inside the second larger vessel, see Fig. 1.

3. Results

In Fig. 2 for each target we show typical time distributions of the measured hits in one layer of the detector in a single antiproton beam pulse. The vertical lines indicate the time interval Δt between 760 and 830 ns where the signals from the $\bar{p}$ annihilations in the targets are expected. We can see that in the Δt interval few hits are present for Ni, Sn and Pt targets, numerous hits for a dummy thick target and no hit is present when no target is placed on the $\bar{p}$ beam (the so-called "empty target").

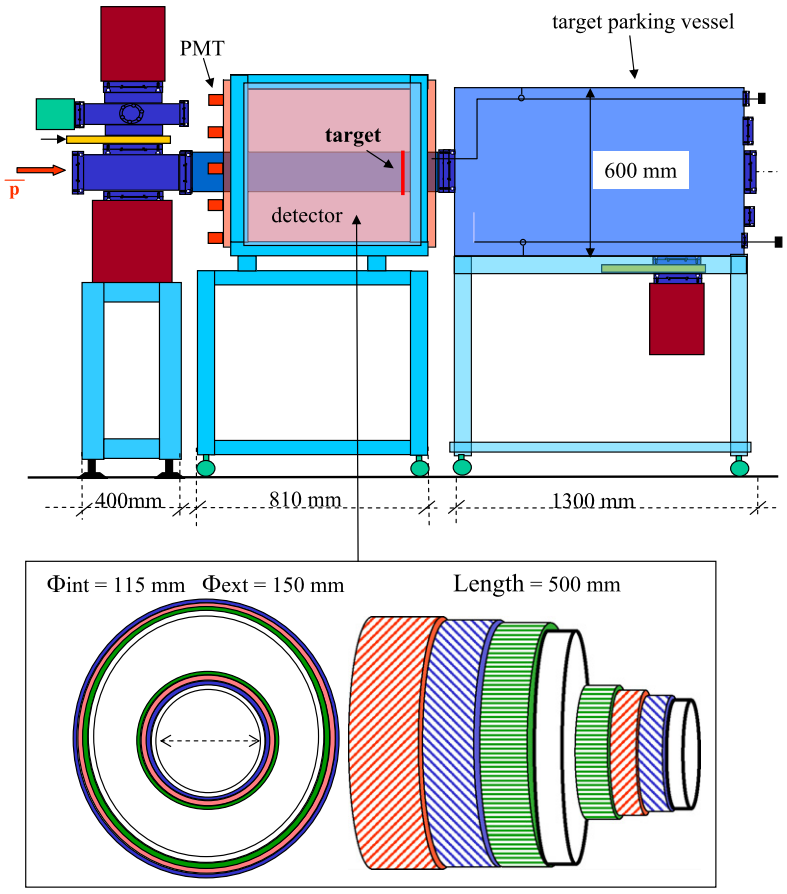

Fig. 1. ASACUSA experimental setup for σ measurement of $\bar{p}$ at 5.3 MeV. The targets are positioned near the parking vessel to avoid signals by antiprotons scattered on the walls. Just to measure Rutherford scattering the target is moved backward (see text).

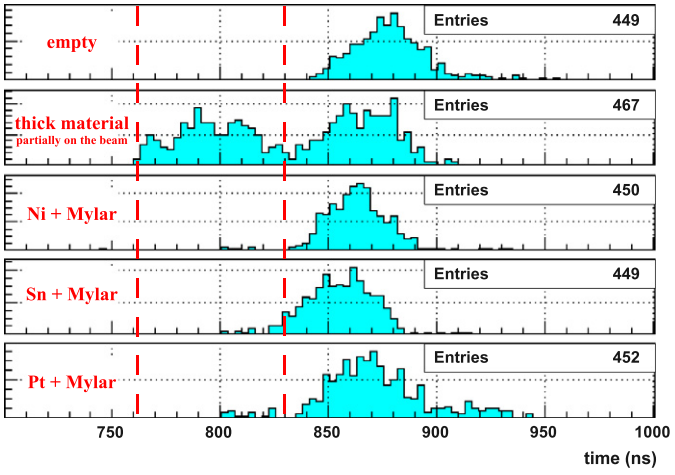

Fig. 2. Time distributions of the signals in one layer of the detector for one antiproton beam pulse with different targets.

After the aforementioned Δt interval the whole detector is fired and saturated by a flux of pions coming from the end wall of the target vessel.

The absence of events before 830 ns with the empty target also indicates that the radial halo of the $\bar{p}$ beam is well confined and that the annihilations from the end wall of the target vessel are well separated in time from the annihilations in the target.

Distributions similar to those of Fig. 2 are achieved simultaneously also with the other 5 layers of the detector. The signals in the Δt interval of all the layers are used to reconstruct the vertices of the annihilations as explained in the previous section. Some hits in the Δt interval, which appear only when the targets are inserted, are not due to pions coming from the target. They can come from the pions emitted by antiprotons annihilations on the lateral wall of the target vessel following antiprotons diffusion from the target. This contamination is however removed when we reconstruct the vertices and we require that they lie at the target position.

For each target the number of the reconstructed vertices has been counted, and the contribution of the Mylar support has been subtracted by using the data acquired with a target consisting of only a bare Mylar foil. The antiproton annihilation cross section can be determined by means of the following formula:

$$\sigma = \frac{N_{ev}}{N_{\bar{p}} N_A \frac{\rho}{M} l \epsilon_{ev}} \tag{1}$$

where N_{ev} is the number of the vertices reconstructed in the target in the fiducial time interval Δt, $N_{\bar{p}}$ is the number of the incident $\bar{p}$s on the target, ρ is the target density, N_A is the Avogadro's number, M is the atomic weight of the target, l is the target thickness, ϵ_{ev} is the vertex detection efficiency.

Using Eq. (1) it is possible to infer the cross section from the number of the reconstructed vertices and from the number of the incident $\bar{p}$s measured by the beam counter.

A fraction of the reconstructed vertices comes from the annihilations on the oxygen atoms contaminating the targets. The RBS analysis we performed indicates that in the case of the Pt target this contribution is negligible while for the Ni and Sn targets it must be considered [15]. By assuming $\sigma = \sigma_0 A^{2/3}$ (that is valid for the high energy regime) and $\sigma = \sigma_0 A^{4/3}$ (which corresponds to a

rough approximation of the $ZA^{1/3}$ valid for the very low energy regime) we have evaluated the percentage of the annihilations on the oxygen contaminants with respect to the metallic targets. With the former model the percentages are about 20% both for Ni and Sn while with the latter model they are about 10%. We have corrected the data by assuming both the models, see later.

In order to determine the mass number (A) dependence of the antiproton annihilation cross section, the Mylar target can also be used. Since it is a compound we cannot use Eq. (1). Taking into account that the macroscopic cross section for one element $\Sigma = N_A \frac{\rho}{M}\sigma$ can be written for a compound as $\Sigma = \frac{N_A \rho \sum_i n_i \sigma_i}{\sum_i n_i M_i}$ where n_i is the proportion by number of the ith element in the material and assuming

$$\sigma = \sigma_0 A^{\alpha} \tag{2}$$

we can introduce an equivalent mass number A_{eq} and an equivalent cross section σ_{eq} for the compound which satisfies Eq. (2) and conserves the Σ value:

$$\frac{\sum_i n_i \sigma_i}{\sum_i n_i A_i} = \frac{\sigma_{eq}}{A_{eq}} \tag{3}$$

Clearly the resulting equivalent mass number

$$A_{eq} = \left[\frac{\sum_i n_i A_i}{\sum_i n_i A_i^{\alpha}}\right]^{\frac{1}{1-\alpha}} \tag{4}$$

is model dependent but in the Mylar case for the expected α values A_{eq} has only a weak dependence on α. For example for the previously mentioned $\alpha = 2/3$ and $\alpha = 4/3$, A_{eq} is 11.2 and 12.4, respectively.

As reported above we cannot use the beam counter to determine the $N_{\bar{p}}$ values since the device has not been calibrated. The recorded signals of the beam counter provides only the relative intensities of the antiprotons fluxes on the different targets and therefore in a first stage we can only determine the annihilation cross sections in respect, for example, to the nickel target assumed as unit. We will indicate this relative annihilation cross section with the symbol σ^* to distinguish this adimensional quantity from the absolute annihilation cross section denoted by the symbol σ.

In Fig. 3 the relative σ^*_{eq} corresponding to $A_{eq} = 11.2$ has been plotted for the Mylar target together with the relative σ^* obtained for the metallic targets as described before with the contaminant subtraction corresponding to $\sigma \sim A^{2/3}$. The shown error bars are the quadratic sums of the statistical and systematic errors. The contribution of the systematic errors is very low and is mainly due to the uncertainties in the targets thicknesses. Another systematical error could come from assuming the same detection efficiency for the different targets and this error can be estimated to be of the order of few percent of the measured values. This can be evaluated by considering that in the present experiment an annihilation event is counted only when a vertex is reconstructed and this occurs only when at least 2 charged tracks are detected. From $\bar{p}$–p annihilation at rest the percentage of only neutral products is of the order of 3% [1], while from the annihilation of $\bar{p}$ on neutron the percentage of events with less than two charged pions is about 16% as evaluated for the deuterium target [1]. So for a target with equal numbers of protons and neutrons we can estimate that the number of undetectable events is about 9–10% of the annihilations and it increases up to 11% in the case of the Pt target due to the different nucleon composition. Then we can conclude that the differences in the lost events are less than 1–2% of the counted events among the used targets. Within this small differences we have assumed the same detection efficiency for the used targets and since the cross sections measurements are relative the number of lost events does not affect their values.

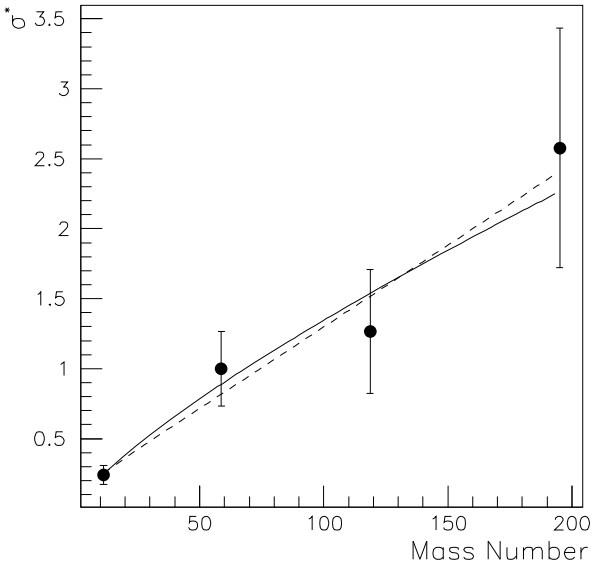

Fig. 3. Antiproton relative annihilation cross section data (σ^*) with the continuous line representing the best fit function cA^{α} (c and α are free parameters) and the dashed line is the best fit of the function $K\sigma$ where K is a free parameter and $\sigma = \pi R^2[1 + \frac{Ze^2(m+M)}{4\pi\epsilon_0 ERM}]$, see text. Here R is parametrized as $1.840 + 1.120\ \mathrm{A}^{1/3}$ fm [7].

In the same plot the best fit of the function cA^{α} to the data is depicted. The fit parameter α results to be 0.78 ± 0.20. If we assume $A_{eq} = 12.4$ and 10% for the contaminants corrections (both coming from $\sigma \sim A^{4/3}$, as commented before), we get again $\alpha = 0.78 \pm 0.20$. The equality of the fit results indicates that the behavior of the measured cross sections is independent within the errors from the assumed model for the evaluation of A_{eq} and the oxygen contaminants.

In Fig. 3 the dashed line is derived from a simple semiclassical model where the black-disk model is extended to include the focusing effect of the Coulomb interaction between the nucleus and the charged antiproton projectile at low energies [7]. This behavior is very close to the best fit function and shows a good agreement with the experimental data.

Besides the measurement of the σ^*, we can also estimate the absolute values of σ by using the scattered antiprotons by Rutherford diffusion. For this purpose the Sn target has been positioned 15 cm upstream in respect to the usual target position in order to increase the number of the annihilations of the scattered antiprotons on the lateral wall of the target vessel which had a diameter of 15 cm. We want to point out that this method is critical with a pulsed beam since the large number of the Rutherford events in respect to the annihilations in the target for heavy nuclei can saturate the data acquisition and we were able to perform this measurement just for the Sn target.

From the knowledge of the Rutherford scattering formula and the measurement of the reconstructed annihilations in a selected $\Delta\theta$ interval it is possible to determine the absolute number of the incident antiprotons ($N_{\bar{p}}$) and then infer the value of the annihilation cross section (σ) from the number of events in the target (N_{ev}). An equivalent method consists of measuring the slope of the linear behavior of the z-coordinate vertex distribution of the Rutherford annihilations on the beam pipe wall.

In fact, starting from the Rutherford differential cross section

$$\frac{d\sigma_{Ruth}}{d\Omega} = \left(\frac{Ze^2}{16\pi\epsilon_0 E}\right)^2 \frac{1}{\sin^4(\frac{\theta}{2})} \tag{5}$$

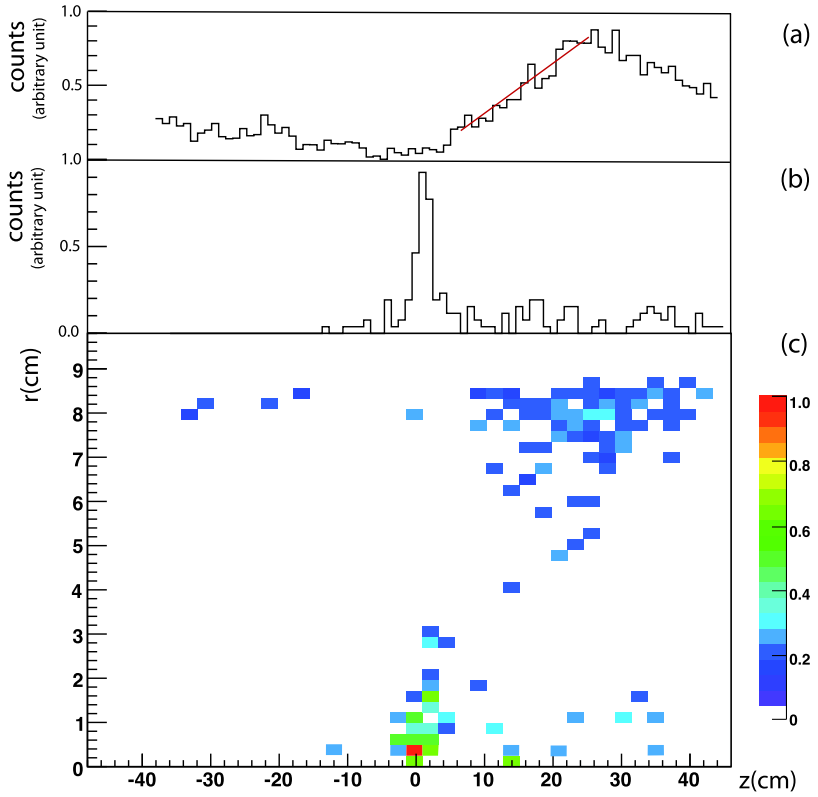

Fig. 4. Reconstructed vertices for the absolute σ measurement. (a) z distribution for the vertices selected on the lateral wall of the target vessel. The red line is the linear fit (notice that also upstream some background is present, which is not uniform in z due to detector properties, but with a much smaller slope); (b) z distribution for the vertices close to the axis of the target vessel (the peak corresponds to the annihilations on the target); (c) radius (r) vs. z of the vertex density distribution. (For interpretation of the references to color in this figure legend, the reader is referred to the web version of this Letter.)

and calling N_{wall} the number of annihilations per unit length over a cylinder of radius R and the axis coincident with the direction, z, of the antiproton beam we can obtain

$$\frac{dN_{wall}}{dz} = N_{\bar{p}} n l Z^2 \frac{\pi}{2} \alpha^2 \left(\frac{\hbar c}{E}\right)^2 \frac{1}{R^2} f\left(\frac{z}{R}\right) \tag{6}$$

$$\text{with} \quad f\left(\frac{z}{R}\right) = \left(\frac{1+2(\frac{z}{R})^2}{\sqrt{1+(\frac{z}{R})^2}} + 2\frac{z}{R}\right) \tag{7}$$

where n is the number density of the target with thickness l.

Since $df/d(\frac{z}{R}) \simeq 4$ for $z \gtrsim R/2$, the number of annihilation vertices for antiprotons scattered from the target downstream increases linearly with the distance from the target, see Fig. 4.

Then from the slope of the fitted straight line it is possible to determine $N_{\bar{p}}$ and thereby the absolute annihilation cross section σ by counting the events in the target. This last number must be corrected for the presence of the Mylar substrate by means of the relative cross section measurement reported above, while the Mylar contribution to the Rutherford-scattered antiprotons is negligible.

Following this procedure we get $\sigma = (4.2 \pm 0.9)$ barn for Sn target. The result is consistent with the expected value from the black-disk model with Coulomb correction ($\sigma = 4.9$ barn) [7]. We must point out that this method is almost completely insensitive to the misalignment of the antiproton beam with respect to the pipe symmetry axis (which was anyway measured, showing that the core of the beam was less than 2 cm off from the pipe axis), and consequently also to the extent of the beam in the x–y plane. We calculated that, by effect of the integration of the Rutherford formula over the azimuthal angle, the effective result differs from the ideal one by a quantity whose leading term is quadratic in $\Delta R/R$, where ΔR is the radial distance between the scattering centre and the geometrical centre of the pipe: in practice, less than 5% in our case, which is a very negligible systematic uncertainty.

In addition the absolute σ values for the Ni and Pt targets can be evaluated from the absolute σ value for Sn together with the relative σ^* values we have reported. The results are $\sigma = (3.3 \pm 1.5)$ barn for Ni and $\sigma = (8.6 \pm 4.1)$ barn for Pt. Clearly they are consistent with the black-disk model with Coulomb correction [7] since, as we have previously mentioned, both the absolute σ for Sn and the relative σ^* values behaviors are in agreement. The errors for Ni and Pt targets are increased in respect to the relative values due to the error propagation.

In Fig. 5 our absolute σ values are plotted with the existing measurements at energies below 500 MeV. It appears evident that at very low energies the present measurements are the only extending to the heavy nuclear targets range.

4. Conclusions

For the first time the $\bar{p}$ annihilation cross sections on medium-heavy and heavy nuclear targets (Mylar, Ni, Sn, Pt) have been measured at low energy (5.3 MeV) by the ASACUSA Collaboration. This represents also the first measurements of the antinucleon annihilation cross section at low energy performed with a pulsed beam.

The results are in agreement with the predictions from the black-disk model with the contribution of the Coulomb interaction between the antiproton and the nucleus at low energies [7].

The results presented here show the usefulness of the applied technique for measurements of the antiproton annihilation cross sections on solid targets and in our apparatus this is possible over

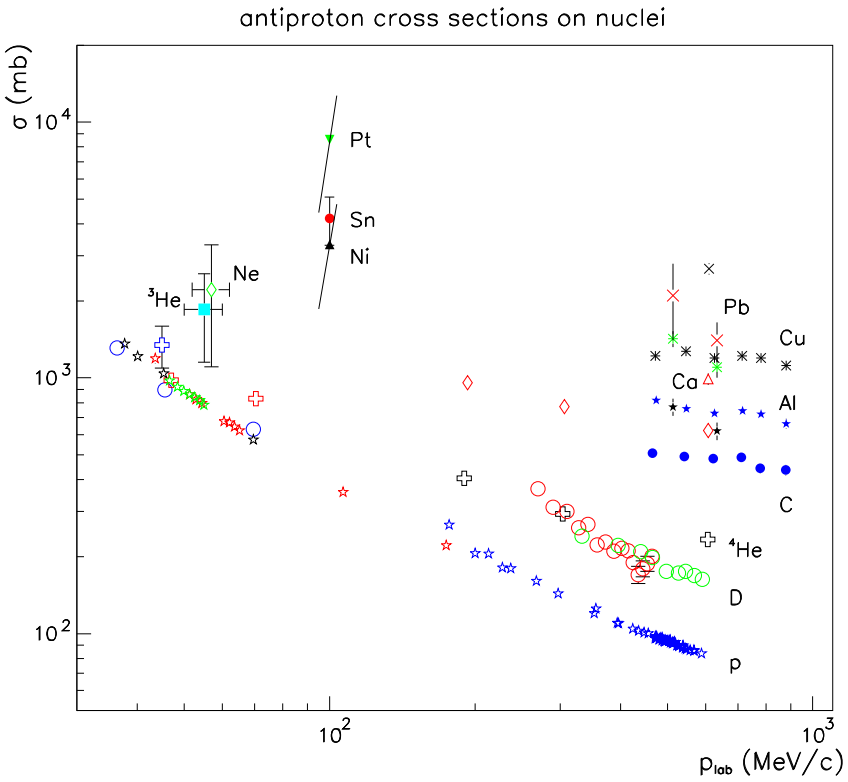

Fig. 5. Comparison among antiproton cross sections measurements at energies below 500 MeV. The symbols for the targets are: ☆ for hydrogen (blue from Ref. [16], red from Ref. [17], green from Ref. [18], black from Ref. [2]), ◯ for deuterium (blue from Ref. [3], red from Ref. [19], green from Ref. [20]), empty cross for ^{4}He (blue from Ref. [21], red from Ref. [3], black from Ref. [22,23]), ■ for ^{3}He (from Ref. [5]), ● for C (from Ref. [24]), ◇ for Ne (green from Ref. [4], red from Ref. [25]), ★ for Al (blue from Ref. [24], black from Ref. [26]), △ for Ca (from Ref. [27]), ∗ for Cu (black from Ref. [24], green from Ref. [26]), × for Pb (red from Ref. [26], black from Ref. [27]), ▲ for Ni (present experiment), • for Sn (present experiment), ▼ for Pt (present experiment). All the data are for annihilation cross section (σ) measurements with the exception of those from Refs. [19,20,22–27] which are for the reaction cross section (σ_r). In the selected $\bar{p}$ lab momentum range, the σ_r values are mainly due to the annihilation process (σ) since the other processes (inelastic scattering, charge exchange, nucleon knock-out) contribute for a few percent only. (For interpretation of the references to color in this figure legend, the reader is referred to the web version of this Letter.)

some orders of magnitude in kinetic energy of the antiprotons. The ASACUSA Collaboration has planned to extend the measurement down to ≈ 100 keV with the addiction of the ASACUSA radio frequency decelerator (RFQD) and with very thin targets supported by a carbon foil.

Acknowledgements

We would like to thank the CERN AD staff and all the other members of the ASACUSA Collaboration for their help and support. Also thanks to Giorgio Di Giovambattista for his help in the computers management. This work was supported by Istituto Nazionale di Fisica Nucleare (INFN), Università di Brescia, the European Young Investigator Awards (EURYI) of the European Science Foundation and the Deutsche Forschungsgemeinschaft (DFG), and the Munich Advanced Photonics (MAP) cluster of DFG.

References

[1] G. Bendiscioli, D. Kharzeev, Riv. Nuovo Cim. 17 (1994) 1.
[2] A. Zenoni, et al., OBELIX Collaboration, Phys. Lett. B 461 (1999) 405.
[3] A. Zenoni, et al., OBELIX Collaboration, Phys. Lett. B 461 (1999) 413.
[4] A. Bianconi, et al., Phys. Lett. B 481 (2000) 194.
[5] A. Bianconi, et al., Phys. Lett. B 492 (2000) 254.
[6] L.D. Landau, E.M. Lifshitz, Quantum Mechanics (Non-Relativistic Theory), Course of Theoretical Physics, vol. 3, Butterworth–Heinemann, 1981.
[7] C.J. Batty, E. Friedman, A. Gal, Nucl. Phys. A 689 (2001) 721.
[8] A. Bianconi, G. Bonomi, E. Lodi Rizzini, L. Venturelli, A. Zenoni, Phys. Rev. C 62 (2000) 014611.
[9] M. Astrua, et al., Nucl. Phys. A 697 (2002) 209.
[10] F. Iazzi, et al., OBELIX Collaboration, Phys. Lett. B 475 (2000) 378.
[11] S. Maury, Hyperf. Interact. 43 (1997) 109.
[12] A. Mozzanica, et al., Nuovo Cim. B 122 (2007) 759.
[13] D. Bolognini, et al., Nucl. Instr. Meth. A 572 (2007) 281.
[14] R. Armenteros, B. French, in: E.H. Burhop (Ed.), $\bar{N}N$ Interactions in High Energy Physics, vol. 4, Academic Press, New York, 1969, p. 237.
[15] M. Corradini, et al., in preparation.
[16] W. Brückner, et al., Z. Phys. A 335 (1990) 217.
[17] A. Bertin, et al., OBELIX Collaboration, Phys. Lett. B 369 (1996) 77.
[18] A. Benedettini, et al., OBELIX Collaboration, Nucl. Phys. B (Proc. Suppl.) 56A (1997) 58.
[19] T.E. Kalogeropoulos, G.S. Tzanakos, Phys. Rev. D 22 (1980) 2585.
[20] R. Bizzarri, et al., Nuovo Cim. A 22 (1974) 225.
[21] F. Balestra, et al., Phys. Lett. B 230 (1989) 36.
[22] F. Balestra, et al., Phys. Lett. B 149 (1984) 69.
[23] F. Balestra, et al., Phys. Lett. B 165 (1985) 265.
[24] K. Nakamura, et al., Phys. Rev. Lett. 52 (1984) 731.
[25] F. Balestra, et al., Nucl. Phys. A 452 (1986) 573.
[26] V. Ashford, et al., Phys. Rev. C 31 (1985) 663.
[27] D. Garreta, et al., Phys. Lett. B 149 (1984) 64.